

REPORT DOCUMENTATION PAGE				Form Approved OMB NO. 0704-0188	
<p>The public reporting burden for this collection of information is estimated to average 1 hour per response, including the time for reviewing instructions, searching existing data sources, gathering and maintaining the data needed, and completing and reviewing the collection of information. Send comments regarding this burden estimate or any other aspect of this collection of information, including suggestions for reducing this burden, to Washington Headquarters Services, Directorate for Information Operations and Reports, 1215 Jefferson Davis Highway, Suite 1204, Arlington VA, 22202-4302. Respondents should be aware that notwithstanding any other provision of law, no person shall be subject to any penalty for failing to comply with a collection of information if it does not display a currently valid OMB control number.</p> <p>PLEASE DO NOT RETURN YOUR FORM TO THE ABOVE ADDRESS.</p>					
1. REPORT DATE (DD-MM-YYYY) 30-07-2010		2. REPORT TYPE Final Report		3. DATES COVERED (From - To) 1-Oct-2009 - 30-Jun-2010	
4. TITLE AND SUBTITLE MODELING AND CONTROL OF A TETHERED ROTORCRAFT				5a. CONTRACT NUMBER W911NF-09-1-0567	
				5b. GRANT NUMBER	
				5c. PROGRAM ELEMENT NUMBER 611102	
6. AUTHORS Nathan Slegers				5d. PROJECT NUMBER	
				5e. TASK NUMBER	
				5f. WORK UNIT NUMBER	
7. PERFORMING ORGANIZATION NAMES AND ADDRESSES University of Alabama - Huntsville Office of Sponsored Programs University of Alabama in Huntsville Huntsville, AL 35899 -				8. PERFORMING ORGANIZATION REPORT NUMBER	
9. SPONSORING/MONITORING AGENCY NAME(S) AND ADDRESS(ES) U.S. Army Research Office P.O. Box 12211 Research Triangle Park, NC 27709-2211				10. SPONSOR/MONITOR'S ACRONYM(S) ARO	
				11. SPONSOR/MONITOR'S REPORT NUMBER(S) 56044-NS.1	
12. DISTRIBUTION AVAILABILITY STATEMENT Approved for Public Release; Distribution Unlimited					
13. SUPPLEMENTARY NOTES The views, opinions and/or findings contained in this report are those of the author(s) and should not be construed as an official Department of the Army position, policy or decision, unless so designated by other documentation.					
14. ABSTRACT A tethered rotorcraft model is developed using a computationally efficient recursive tether model. The recursive rigid-body tether model results in unconstrained ordinary differential equations and maintains much of the simplicity of simple lumped mass tether models while avoiding numerical difficulties associated with using many stiff elastic elements with low mass. Further efficiency is achieved by treating each tether link as a body of revolution and assuming that tether spin is negligible to the dynamics. The tether is attached to a 6 degree of					
15. SUBJECT TERMS Unmanned Air Vehicles, Rotorcraft, Tether					
16. SECURITY CLASSIFICATION OF:			17. LIMITATION OF ABSTRACT UU	15. NUMBER OF PAGES	19a. NAME OF RESPONSIBLE PERSON Nathan Slegers
a. REPORT UU	b. ABSTRACT UU	c. THIS PAGE UU			19b. TELEPHONE NUMBER 256-824-6543

Report Title

MODELING AND CONTROL OF A TETHERED ROTORCRAFT

ABSTRACT

A tethered rotorcraft model is developed using a computationally efficient recursive tether model. The recursive rigid-body tether model results in unconstrained ordinary differential equations and maintains much of the simplicity of simple lumped mass tether models while avoiding numerical difficulties associated with using many stiff elastic elements with low mass. Further efficiency is achieved by treating each tether link as a body of revolution and assuming that tether spin is negligible to the dynamics. The tether is attached to a 6 degree of freedom rotorcraft model using a single visco-elastic element. The final recursive tether-rotorcraft model is well suited for a variety of trade studies required for design and analysis of such systems due to its low computational cost and numerical robustness. Simulations are used to show how the proposed recursive model can be used to investigate the dynamic response and tether loads for a small 3 kg tethered rotorcraft.

List of papers submitted or published that acknowledge ARO support during this reporting period. List the papers, including journal references, in the following categories:

(a) Papers published in peer-reviewed journals (N/A for none)

Number of Papers published in peer-reviewed journals: 0.00

(b) Papers published in non-peer-reviewed journals or in conference proceedings (N/A for none)

Number of Papers published in non peer-reviewed journals: 0.00

(c) Presentations

Number of Presentations: 0.00

Non Peer-Reviewed Conference Proceeding publications (other than abstracts):

Number of Non Peer-Reviewed Conference Proceeding publications (other than abstracts): 0

Peer-Reviewed Conference Proceeding publications (other than abstracts):

Number of Peer-Reviewed Conference Proceeding publications (other than abstracts): 0

(d) Manuscripts

Number of Manuscripts: 0.00

Patents Submitted

Patents Awarded

Graduate Students

<u>NAME</u>	<u>PERCENT SUPPORTED</u>
FTE Equivalent:	
Total Number:	

Names of Post Doctorates

<u>NAME</u>	<u>PERCENT SUPPORTED</u>
FTE Equivalent:	
Total Number:	

Names of Faculty Supported

<u>NAME</u>	<u>PERCENT SUPPORTED</u>	National Academy Member
Nathan Slegers	0.30	No
FTE Equivalent:	0.30	
Total Number:	1	

Names of Under Graduate students supported

<u>NAME</u>	<u>PERCENT SUPPORTED</u>
FTE Equivalent:	
Total Number:	

Student Metrics

This section only applies to graduating undergraduates supported by this agreement in this reporting period

The number of undergraduates funded by this agreement who graduated during this period: 0.00

The number of undergraduates funded by this agreement who graduated during this period with a degree in science, mathematics, engineering, or technology fields:..... 0.00

The number of undergraduates funded by your agreement who graduated during this period and will continue to pursue a graduate or Ph.D. degree in science, mathematics, engineering, or technology fields:..... 0.00

Number of graduating undergraduates who achieved a 3.5 GPA to 4.0 (4.0 max scale):..... 0.00

Number of graduating undergraduates funded by a DoD funded Center of Excellence grant for Education, Research and Engineering:..... 0.00

The number of undergraduates funded by your agreement who graduated during this period and intend to work for the Department of Defense 0.00

The number of undergraduates funded by your agreement who graduated during this period and will receive scholarships or fellowships for further studies in science, mathematics, engineering or technology fields: 0.00

Names of Personnel receiving masters degrees

<u>NAME</u>
Total Number:

Names of personnel receiving PhDs

<u>NAME</u>

Total Number:

Names of other research staff

<u>NAME</u>

<u>PERCENT SUPPORTED</u>

FTE Equivalent:

Total Number:

Sub Contractors (DD882)

Inventions (DD882)

FINAL TECHNICAL REPORT

W911NF-09-1-0567

MODELING AND CONTROL OF A TETHERED ROTORCRAFT

by:

Nathan Slegers
University of Alabama in Huntsville
Huntsville, Alabama

A tethered rotorcraft model is developed using a computationally efficient recursive tether model. The recursive rigid-body tether model results in unconstrained ordinary differential equations and maintains much of the simplicity of simple lumped mass tether models while avoiding numerical difficulties associated with using many stiff elastic elements with low mass. Further efficiency is achieved by treating each tether link as a body of revolution and assuming that tether spin is negligible to the dynamics. The tether is attached to a 6 degree of freedom rotorcraft model using a single visco-elastic element. The final recursive tether-rotorcraft model is well suited for a variety of trade studies required for design and analysis of such systems due to its low computational cost and numerical robustness. Simulations are used to show how the proposed recursive model can be used to investigate the dynamic response and tether loads for a small 3 kg tethered rotorcraft.

Nomenclature

a	= lift curve slope of the main rotor.
\mathbf{a}_j^c	= acceleration of j^{th} connection joint with respect to the inertial frame
\mathbf{a}_j^m	= acceleration of mass center of j^{th} link with respect to the inertial frame
b_j	= j^{th} link of the tether (ground link $j = 0$, root link $j = 1$, parent body $j = jp$)
c_j	= j^{th} connection joint (ground connection joint $j = 0$)
c_{MR}	= main rotor chord.
c_T	= tether connection to rotorcraft
C_{DX}, C_{DY}, C_{DZ}	= fuselage drag coefficients.
C_{Dj}	= tether drag coefficient
C_S	= tether damping coefficient
C_v	= viscous damping coefficient
d	= diameter of the tether
\mathbf{E}_n	= $n \times n$ identity matrix
$\mathbf{F}_A, \mathbf{M}_A$	= rotorcraft aerodynamic forces and moments
\mathbf{F}_{Dj}	= drag force for j^{th} link
\mathbf{F}_T, F_T	= visco-elastic element tension vector and magnitude
\mathbf{F}_{FUS}	= drag from fuselage
$\mathbf{F}_{MR}, \mathbf{M}_{MR}$	= main rotor force and moment
$\mathbf{F}_{TR}, \mathbf{M}_{TR}$	= tail rotor force and moment
\mathbf{F}_j	= 5×1 force matrix for j^{th} link
\mathbf{F}_W	= rotorcraft weight
$\mathbf{i}_B, \mathbf{j}_B, \mathbf{k}_B$	= rotorcraft body frame unit vectors
$\mathbf{i}_I, \mathbf{j}_I, \mathbf{k}_I$	= inertial frame unit vectors
\mathbf{I}_B	= rotorcraft inertia matrix
I_{nn}	= mass moment of inertia about i, j, k body axes with $n = x, y, z$ respectively
\mathbf{I}_j	= inertia matrix of j^{th} body
$\tilde{\mathbf{I}}_j$	= 2×2 link inertia matrix consisting of I_{yy} and I_{zz}
k	= rotor head stiffness
K_{LAT}, K_{LON}	= steady state flapping gains
K_s, K_v	= static and viscous stiffness
\mathbf{L}_j	= moment in j^{th} connection joint acting on the $j+1$ link and the j^{th} link respectively
$\tilde{\mathbf{L}}_j$	= 2×1 moment vector consisting of \mathbf{j} and \mathbf{k} components of \mathbf{L}_j
L_{nj}	= n^{th} component of \mathbf{L}_j with $n = x, y, z$ respectively
L_{ve}	= visco-elastic element unstretched length
l_j	= length of individual j^{th} link
l_T	= overall tether length
m_B	= rotorcraft mass
m_j	= mass of link j
m_T	= total mass of the tether
N	= total number of tether links
p_B, q_B, r_B	= rotorcraft angular velocity components
p_j, q_j, r_j	= angular velocity components of the j^{th} link
$q_{0j}, q_{1j}, q_{2j}, q_{3j}$	= quaternion parameters for j^{th} link
\mathbf{r}_j^m	= position vector from connection joint $j-1$ to mass center j
\mathbf{r}_j^c	= position vector from connection joint $j-1$ to connection joint j

\mathbf{r}_{cg}^{ct}	= position from the rotorcraft mass center to c_T
R_{MR}	= main rotor radius
\mathbf{R}_j	= reaction in j^{th} connection joint acting on the $j+1$ link and the j^{th} link respectively
$\hat{\mathbf{S}}_j^c$	= 2 x 3 sub matrix of skew symmetric cross product operator for position vector for \mathbf{r}_j^c
$\hat{\mathbf{S}}_j^m$	= 2 x 3 sub matrix of skew symmetric cross product operator for position vector for \mathbf{r}_j^m
$\tilde{\mathbf{S}}_j^m$	= 2 x 2 sub matrix for skew symmetric cross product operator for position vector \mathbf{r}_j^m
s_j	= frontal area of j^{th} link
s_{ve}	= visco-elastic element stretch
T_{TR}	= tail rotor thrust
\mathbf{T}_I^B	= transformation from inertial to rotorcraft body frame
\mathbf{T}_I^j	= transformation from inertial to j^{th} body frame
\mathbf{T}_{j-1}^j	= transformation from the $j-1$ body frame to the j^{th} body frame
$\hat{\mathbf{T}}_{j-1}^j$	= 2 x 2 sub matrix of the second and third columns of the second and third rows of \mathbf{T}_{j-1}^j
$\tilde{\mathbf{T}}_{j-1}^j$	= 1 x 2 sub matrix of the second and third elements of the first row of \mathbf{T}_{j-1}^j
u, v, w	= rotorcraft body velocity components
u_w, v_w, w_w	= wind velocity components
u_{lat}, u_{lon}	= lateral and longitudinal swash plate controls
u_{col}	= main rotor collective pitch control.
\mathbf{V}, V	= rotorcraft velocity vector and magnitude
\mathbf{V}_j	= mass center velocity of the j^{th} link
$\dot{\mathbf{v}}_j$	= 5 x 1 acceleration vector consisting components of $\tilde{\boldsymbol{\alpha}}_{j/I}$ and $\boldsymbol{\alpha}_{j-1}^c$ respectively
V_{TIP}	= main rotor tip speed.
\mathbf{W}_j	= weight of j^{th} link
x_{cj}, x_{mj}	= length from $j-1$ connection to the j^{th} connection and mass center
α	= longitudinal main rotor flapping angle
β	= lateral main rotor flapping angle
$\boldsymbol{\alpha}_{j/I}$	= angular acceleration vector of j^{th} with respect to the inertial frame
$\tilde{\boldsymbol{\alpha}}_{j/I}$	= 2 x 1 angular acceleration vector consisting of \mathbf{j} and \mathbf{k} components of $\boldsymbol{\alpha}_{j/I}$
$\Delta x, \Delta y, \Delta z$	= visco-elastic element displacement
τ	= rotor time constant
$\boldsymbol{\omega}_B$	= rotorcraft angular velocity vector
$\boldsymbol{\omega}_{j/I}$	= angular velocity vector of j^{th} link with respect to the inertial frame
$\boldsymbol{\omega}_{jj-1}$	= relative angular velocity of j^{th} link with respect to the $j-1$ link
$\dot{\boldsymbol{\omega}}_j$	= 2 x 1 angular acceleration vector consisting of the j and k components of $\dot{\boldsymbol{\omega}}_{j/j-1}$
$\tilde{\boldsymbol{\omega}}_{j/I}$	= 2 x 1 angular velocity vector consisting of j and k components of $\boldsymbol{\omega}_{j/I}$
ω_{nj}	= n^{th} component of $\boldsymbol{\omega}_{jj-1}$ with $n = x, y, z$ respectively
Ω_{MR}	= main rotor angular velocity
$\varphi_B, \theta_B, \psi_B$	= rotorcraft Euler angles
$\varphi_j, \theta_j, \psi_j$	= j^{th} link Euler angles
ρ	= atmospheric density

I. Introduction

FINDING, tracking, and monitoring events and activities of interest on a continuous basis are critically important for intelligence, surveillance, and reconnaissance (ISR). In particular it is desirable to monitor large areas of greater than ten square kilometers with either radar or high resolution cameras for distinguishing and tracking people and vehicles. In addition, it is desirable to monitor these areas on a persistent basis using unmanned autonomous systems (UAS). Another key component in ISR is the communications-relay platform. Traditional mast-mounted antennas are limited in range and constrain the commander to available terrain. With a traditional mast-mounted antenna in typical terrain about 2,800 km² of battle space is covered. Line-of-sight coverage in the same terrain for an antenna at 300 m AGL covers about 31,000 km², more than 10 times the mast-mounted antenna coverage.

The concept of persistent surveillance as a transformational capability has circulated within the Department of Defense for many years. Persistent surveillance, also known as persistent intelligence, surveillance, and reconnaissance (ISR), is an often-used term to describe the need for future ISR capabilities to qualitatively transform intelligence support to operational and tactical commands. The idea surfaces in many forms, including defense program reviews and congressional testimony. Each expression envisions a system achieving near-perfect knowledge and removing uncertainty in war. Persistence means that when global, theater, or local reconnaissance finds something of intelligence or actionable interest, ISR systems, including processing and analytic systems, maintain constant, enduring contact with the target. This increases understanding about the target, which enables a faster decision cycle at all levels of command and supports the application of precision force to achieve desired effects.

Conventional tethered aerostats support both portions of ISR missions: providing high-resolution imagery to ground installations, and providing communications and data-relay to wide areas over any terrain. Unlike fixed-wing aircraft or helicopters, aerostats are lighter-than-air (LTA) typically using helium to stay aloft and are tethered to the ground, by a cable that also provides power. The most well established LTA program today is the Tethered Aerostat Radar System (TARS) that has been operating since 1980 at sites along the southern U.S. border. Each 71 m aerostat, can lift radar or other sensors to a height of 3.5 km, and detect targets out to 500 km. The aerostat can theoretically stay aloft for days at a time and carries the AN/DPS-5 S-band and AN/TPS-63 search radars. Endurance is limited by airborne fuel powering the radar's generator.

The Joint Land Attack Cruise Missile Defense Elevated Netted Sensor System (JLENS) uses the same 71 m TARS aerostat platform for the cruise-missile-defense radars being developed. Each JLENS system consists of two aerostats, one containing a broad area surveillance radar (SuR) to detect cruise missiles and the other a precision radar (PTIR) to track the cruise missile with sufficient precision to guide an intercepting weapon. Following initial threat detection by the SuR, the PTIR takes over to generate a fire solution for available surface-to-air missiles. JLENS is seen by some as the centerpiece of a larger attempt to seamlessly link together numerous sensors across services to build a "single integrated air picture," that will enable effective cruise missile defense. The US Army has also deployed a 17m Rapid Aerostat Initial Development (RAID) for Operation Enduring Freedom in 2001. The RAID system is essentially a much smaller version of JLENS operating at approximately 300m, has a payload of 90 kg, and provides short-range area surveillance and early warning against attacks with small arms, rockets and mortars.

Although the aerostat programs provide low-cost surveillance, they are dependent on weather conditions. One of the most severe limitations is they must be brought to ground in high winds. Specific flying weather restrictions are established for each system ensuring safe flight. Operating characteristics of aerostats also depend on base altitude and temperature. For example, on a cool day stationed at sea level, the aerostat will fly higher than on a warm day stationed at 4,000 mean sea level. The typical endurance is around 15 days, the time when helium refilling is required, but effective endurance is often limited by being grounded in high winds. Another significant limitation of tethered aerostats is their mobility; even the smaller 15-meter RAID is cumbersome to move.

This report develops a small tethered electric rotorcraft as an attractive alternative to a tethered aerostat. A tethered rotorcraft could be either a conventional main rotor and tail configuration or four

rotor system. In either case the footprint would be significantly smaller than an aerostat of similar payload. The tether would be used to provide power to the system and as a high speed fiber optic communication link. A substantial benefit of a small tethered rotorcraft over aerostats is the ability to fly in high winds. A small tethered rotorcraft provides a small, highly mobile, inexpensive platform which can be used for both persistent ISR and as a data-relay.

Modeling of tethered systems has been proposed for a variety of systems including: 2-D analysis of aerostats in response to vertical gusts [1], tethered high altitude balloons [2], and tri-tethered systems [3,4]. In all cases, the aerostat has a similar model which includes aerodynamics, buoyancy, and apparent mass while significantly different approaches are taken in modeling the tether. While the tether is continuous, it is often modeled using discrete elements. The simplest tether models use lumped mass bodies connected with elastic elements [3,4] where each mass has only three degrees of freedom (DOF). A similar lumped mass approach was used by Frost and Costello [5] when modeling connected munitions. A limitation of the simple lumped mass model is that for stiff tethers, the elastic elements must also be stiff to mimic low strain resulting in potentially high frequency vibrations. Addition of a visco-elastic element in [6] improves performance of the lumped mass model for stiff tethers while also adding an extra state for each visco-elastic element. Regardless of which element is used, elastic or visco-elastic, the lumped mass models are appealing because they result in extremely simple, computationally efficient models, even for large numbers of elements. Tether modeling complexity is increased in [2] where beam elements are used rather than lumped masses. Using beam elements allows modeling of bending moments but requires a finite element nonlinear solver so the computational burden is much higher than the lumped mass models. Similarly, Ref. [1] uses a more complex 2-D model where tether elements are modeled as partial differential equation requiring an implicit finite difference algorithm coupled with a Newton-Raphson iterative scheme for a solution.

Tethered rotorcrafts typically result in low tension in the tethers limited by the thrust. Often the tether is comprised of a conductive core, either copper or aluminum, and a fiber optic cable. Strength of the tether is usually sufficient so that limitations in strain on fiber optics are not exceeded, resulting in the tether strain being small compared to the tether sway and surge. This report models the tether using a chain of N bodies connected by spherical joints rather than using stiff elastic elements and lumped masses. The proposed model results in unconstrained ordinary differential equations and maintains much of the simplicity of the lumped mass models while eliminating the numerical problems associated with extremely stiff elastic elements. The tether model takes the form of an open chain common to multi-body dynamics which can be solved using either an order N^3 method by inverting a system mass matrix [7,8] or by recursive rigid-body dynamics which is order N [9]. The later approach is taken here because as shown in [10] the order N method is more computationally efficient as the number of bodies N increases. Computations are further decreased by treating each link as a body of revolution and assuming that tether spin is negligible to the dynamics where each link then only has two degrees of freedoms. The proposed recursive rigid-body tether formulation results in computations on the same order as the three degree of freedom lumped mass models. Furthermore, elimination of high stiffness elements allows larger integration time steps further improving computation speeds. The efficient recursive tether model is coupled to the rotorcraft by a single visco-elastic element. The proposed efficient recursive tether-rotorcraft model is well suited for a variety of trade studies required for design and analysis due to its low computational cost and numerical robustness. As a result, the proposed model can be considered a supplement to alternative approaches requiring an iterative scheme to solve partial differential equations [1] and a finite element nonlinear solver [2] where the computational burden may be prohibitive when running large numbers of simulations for trade studies.

II. System Description

The tether is divided into N bodies connected by spherical joints with each link being a body of revolution. Figure 1 shows the tether attached to the ground with the j^{th} body, b_j , having two connections, joints c_{j-1} and c_j . The N^{th} body, b_N , is the tether terminal link, body b_1 is the root link, where connection c_0 is stationary. Connection c_0 is attached to a fixed or inertial frame (I) defined by three orthogonal unit

vectors, \mathbf{i}_l , \mathbf{j}_l , and \mathbf{k}_l . A link reference frame is assigned to each link as shown with the origin at the link's mass center and \mathbf{i}_j along the axis of revolution with \mathbf{j}_j and \mathbf{k}_j defined to form an orthogonal triad. An rotorcraft body frame with unit vectors \mathbf{i}_B , \mathbf{j}_B , and \mathbf{k}_B is located at the rotorcraft mass center with \mathbf{i}_B aligned with the rotorcraft's longitudinal axis and \mathbf{k}_B in the vertical plane of symmetry. The rotorcraft and tether are connected by a single visco-elastic element from the rotorcraft harness connection c_T to tether terminal connection c_N .

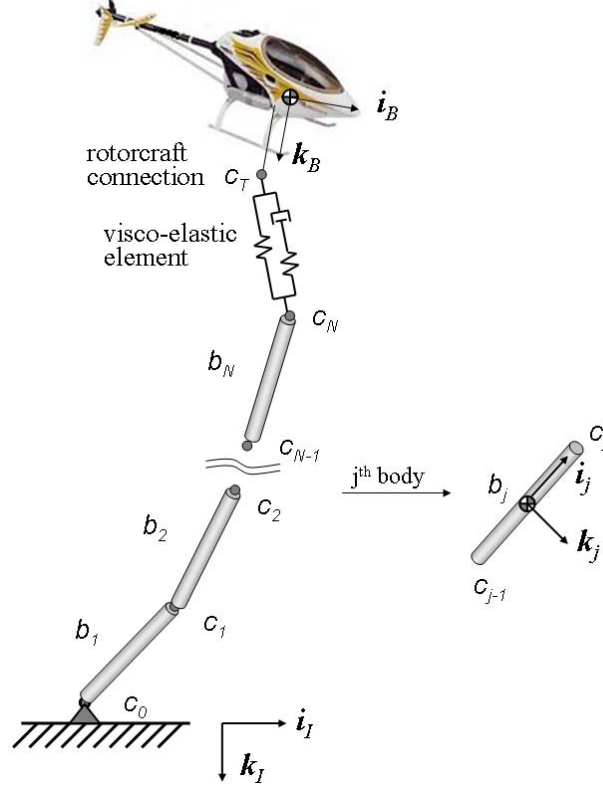


Figure 1. Tethered rotorcraft schematic.

Orientation of the rotorcraft is defined by a sequence of three body-fixed rotations. Starting from the inertial frame, the body frame is defined by rotations about the \mathbf{k} , \mathbf{j} , and \mathbf{i} axes by angles ψ_B , θ_B , and ϕ_B , respectively resulting in the transformation from the inertial frame, I , to the B frame

$$\mathbf{T}_I^B = \begin{bmatrix} c_{\theta_B} c_{\psi_B} & c_{\theta_B} s_{\psi_B} & -s_{\theta_B} \\ s_{\phi_B} s_{\theta_B} c_{\psi_B} - c_{\phi_B} s_{\psi_B} & s_{\phi_B} s_{\theta_B} s_{\psi_B} + c_{\phi_B} c_{\psi_B} & s_{\phi_B} c_{\theta_B} \\ c_{\phi_B} s_{\theta_B} c_{\psi_B} + s_{\phi_B} s_{\psi_B} & c_{\phi_B} s_{\theta_B} s_{\psi_B} - s_{\phi_B} c_{\psi_B} & c_{\phi_B} c_{\theta_B} \end{bmatrix} \quad (1)$$

where $\sin(\chi) = s_\chi$, $\cos(\chi) = c_\chi$. Similarly, orientation of the j^{th} link frame is defined by a sequence of three body-fixed rotations where the j^{th} body frame is defined by rotations about the \mathbf{k} , \mathbf{j} , and \mathbf{i} axes by angles ψ_j , θ_j , and ϕ_j , respectively. In order to avoid a singularity in the rotation kinematics, the link orientation can alternatively be defined by the four quaternion parameters q_{0j} , q_{1j} , q_{2j} , and q_{3j} [11] resulting in the transformation from the inertial frame, I , to the j frame given by

$$\mathbf{T}_I^j = \begin{bmatrix} 2q_{0j}^2 - 1 + 2q_{1j}^2 & 2q_{1j}q_{2j} + 2q_{0j}q_{3j} & 2q_{1j}q_{3j} - 2q_{0j}q_{2j} \\ 2q_{1j}q_{2j} - 2q_{0j}q_{3j} & 2q_{0j}^2 - 1 + 2q_{2j}^2 & 2q_{2j}q_{3j} + 2q_{0j}q_{1j} \\ 2q_{1j}q_{3j} + 2q_{0j}q_{2j} & 2q_{2j}q_{3j} - 2q_{0j}q_{1j} & 2q_{0j}^2 - 1 + 2q_{3j}^2 \end{bmatrix} \quad (2)$$

where

$$\begin{aligned} q_{0j} &= \cos\left(\frac{\psi_j}{2}\right)\cos\left(\frac{\theta_j}{2}\right)\cos\left(\frac{\phi_j}{2}\right) + \sin\left(\frac{\psi_j}{2}\right)\sin\left(\frac{\theta_j}{2}\right)\sin\left(\frac{\phi_j}{2}\right) \\ q_{1j} &= \cos\left(\frac{\psi_j}{2}\right)\cos\left(\frac{\theta_j}{2}\right)\sin\left(\frac{\phi_j}{2}\right) - \sin\left(\frac{\psi_j}{2}\right)\sin\left(\frac{\theta_j}{2}\right)\cos\left(\frac{\phi_j}{2}\right) \\ q_{2j} &= \cos\left(\frac{\psi_j}{2}\right)\sin\left(\frac{\theta_j}{2}\right)\cos\left(\frac{\phi_j}{2}\right) + \sin\left(\frac{\psi_j}{2}\right)\cos\left(\frac{\theta_j}{2}\right)\sin\left(\frac{\phi_j}{2}\right) \\ q_{3j} &= \sin\left(\frac{\psi_j}{2}\right)\cos\left(\frac{\theta_j}{2}\right)\cos\left(\frac{\phi_j}{2}\right) - \cos\left(\frac{\psi_j}{2}\right)\sin\left(\frac{\theta_j}{2}\right)\sin\left(\frac{\phi_j}{2}\right) \end{aligned} \quad (3)$$

A transformation from the $j-1$ frame to the j frame can be formed using (2) and is given as

$$\mathbf{T}_{j-1}^j = (\mathbf{T}_j^I)^T \mathbf{T}_{j-1}^I \quad (4)$$

Position vectors from the $j-1$ connection to the j^{th} body mass center are conveniently expressed in the b_j frame as $\mathbf{r}_j^m = x_{mj} \mathbf{i}_j$. Similarly, the vector from connection $j-1$ to connection j , also expressed in the b_j frame is defined as $\mathbf{r}_j^c = x_{cj} \mathbf{i}_j$. Both vectors, \mathbf{r}_j^m and \mathbf{r}_j^c , have only an \mathbf{i}_j component as a result of each body's symmetry.

III. Rotorcraft Model

The rotorcraft is modeled as a rigid 6 DOF body including three inertial positions of the rotorcraft mass center, x , y , z and the three Euler angles ψ_B , θ_B , and ϕ_B . Body frame velocity components of the rotorcraft mass center are u , v , w while ω_B , the angular velocity of the rotorcraft also in the body frame has components p_B , q_B , r_B . Forces and moments acting on the rotorcraft come from weight, aerodynamic forces from the main rotor, tail rotor and fuselage, and the visco-elastic connection from the rotorcraft harness to the tether.

A. Rotorcraft Forces and Moments

Weight contribution is given below in Eq. (5) while fuselage drag is provided in Eq. (6).

$$\mathbf{F}_W = m_B g \begin{Bmatrix} -s_{\theta_B} \\ s_{\phi_B} c_{\theta_B} \\ c_{\phi_B} c_{\theta_B} \end{Bmatrix} \quad (5)$$

$$\mathbf{F}_{\text{FUS}} = -\frac{1}{2} \rho V_A S \begin{Bmatrix} C_{DX} u \\ C_{DY} v \\ C_{DZ} w \end{Bmatrix} \quad (6)$$

Forces from the main and tail rotors are generated though the four control inputs u_{lat} , u_{lon} , u_{col} and T_{TR} . Tilting of the main rotor is achieved through lateral and longitudinal movement of the swash plate by u_{lat} and u_{lon} . Thrust of the main rotor is controlled through collective pitch u_{col} while thrust of the tail rotor T_{TR} is used directly as a control variable. Thrust from the main rotor can be described as:^{12,13}

$$T_{MR} = \rho (\Omega_{MR} R_{MR})^2 \pi R_{MR}^2 C_T \quad (7)$$

where, the thrust coefficient C_T can be found by solving (8) and (9) using an iterative gradient descent method.

$$C_T = \frac{a\sigma}{2} \left(u_{col} \left(\frac{1}{3} + \frac{\mu^2}{2} \right) + \frac{\mu_z - \lambda}{2} \right) \quad (8)$$

$$\lambda = \frac{C_T}{2\sqrt{\mu^2 + (\lambda - \mu_z)^2}} \quad (9)$$

Where,

$$\mu = \frac{\sqrt{(u - u_w)^2 + (v - v_w)^2}}{V_{TIP}} \quad (10)$$

$$\mu_z = \frac{w - w_w}{V_{TIP}} \quad (11)$$

$$\sigma = 2c_{MR} / \pi R_{MR} \quad (12)$$

Tail rotor thrust is defined in a similar manner as the main rotor thrust.

Lateral and longitudinal control cause cyclic changes in the main rotor blade pitch resulting in the blades flapping creating moments and differential lift. It has been shown that the two first-order flapping equations in (13) and (14) can accurately represent the dynamic motion^{12,13}

$$\dot{\alpha} = -q - \frac{\alpha}{\tau} + \frac{1}{\tau} \left(\frac{\partial \alpha}{\partial \mu_x} \frac{u - u_w}{V_{TIP}} \right) + \frac{K_{LON}}{\tau} u_{LON} \quad (13)$$

$$\dot{\beta} = -p - \frac{\beta}{\tau} + \frac{1}{\tau} \left(\frac{\partial \beta}{\partial \mu_y} \frac{v - v_w}{V_{TIP}} \right) + \frac{K_{LAT}}{\tau} u_{LAT} \quad (14)$$

where, K_{LAT} and K_{LON} are gains describing the resulting steady state flapping angles from a lateral and longitudinal swash plate input, τ is the rotor time constant and:

$$\mu_x = \frac{u - u_w}{V_{TIP}} \quad (15)$$

$$\mu_y = \frac{v - v_w}{V_{TIP}} \quad (16)$$

The thrust of the main and tail rotors in the helicopter reference frame can then be written as,

$$\mathbf{F}_{MR} = \begin{Bmatrix} -T_{MR} s_\alpha \\ T_{MR} s_\beta \\ -T_{MR} (1 - s_\alpha^2 - s_\beta^2) \end{Bmatrix} \quad (17)$$

$$\mathbf{F}_{TR} = \begin{Bmatrix} 0 \\ -T_{TR} \\ 0 \end{Bmatrix} \quad (18)$$

Moments from the main rotor have contributions from motor torque, tilting of the thrust vector and rotor hub stiffness. Torque from the motor can be expressed as a pure yawing moment in the rotor frame as

$$\tilde{N}_{MR} = \rho (\Omega_{MR} R_{MR})^2 \pi R_{MR}^3 C_Q \quad (19)$$

$$C_Q = C_T (\lambda - \mu_z) + \frac{C_D \sigma}{8} \left(1 + \frac{7}{3} \mu^2 \right) \quad (20)$$

Torsional stiffness of the rotor head is modeled as a linear torsional spring with stiffness k . Tilting of the thrust vector from the flapping angles results in pitching and yawing moments. Combining all moments from the main rotor and expressing in the helicopter reference frame results in

$$\mathbf{M}_{MR} = \begin{Bmatrix} -s_\alpha \tilde{N}_{MR} \\ k\beta + s_\beta T_{MR} h_z + s_\beta \tilde{N}_{MR} \\ k\alpha + s_\alpha T_{MR} h_z + (1 - s_\alpha^2 - s_\beta^2) \tilde{N}_{MR} \end{Bmatrix} \quad (21)$$

The tail rotor generates a yawing moment from the tail thrust being behind the mass center.

$$\mathbf{M}_{TR} = \begin{Bmatrix} 0 \\ -T_{TR} h_{tr} \\ 0 \end{Bmatrix} \quad (22)$$

B. Visco-elastic link

The visco-elastic element connecting the rotorcraft and tether is comprised of a spring with static stiffness K_s in parallel with a viscous spring of stiffness K_v and viscous damper with damping coefficient C_v . Visco-elastic line force is written in terms of components Δx , Δy , and Δz , of the difference vector formed by subtracting the inertial position of the rotorcraft connection c_T and the tether connection c_N . Stretch of the visco-elastic element becomes $s_{ve} = \sqrt{\Delta x^2 + \Delta y^2 + \Delta z^2}$ and the stretch rate is \dot{s}_{ve} . Using the difference vector components, the line force vector is written as

$$\mathbf{F}_T = \frac{F_T}{s_{ve}} \begin{Bmatrix} \Delta x \\ \Delta y \\ \Delta z \end{Bmatrix} \quad (23)$$

Equation (24) provides the differential equation for the visco-elastic internal force F_T in terms of the stretch and stretch rate with L_{ve} being the unstretched length.

$$\dot{F}_T + \frac{K_v}{C_v} F_T = \begin{cases} (K_v + K_s) \dot{s}_{ve} + \frac{K_v K_s}{C_v} (s_{ve} - L_{ve}), & s_{ve} - L_{ve} > 0 \\ 0 & s_{ve} - L_{ve} \leq 0 \end{cases} \quad (24)$$

The first condition in (24) represents the visco-elastic element in tension while the second represents the slack case where the internal force decays to zero.

C. Rotorcraft Dynamic Equations

Final dynamic equations are formed by summing forces and moments about the system CG both in the rotorcraft body reference frame and equating to the time derivative of linear and angular momentum respectively.

$$\begin{Bmatrix} \dot{u} \\ \dot{v} \\ \dot{w} \end{Bmatrix} = \frac{1}{m_B} \left(\mathbf{F}_W + \mathbf{F}_{MR} + \mathbf{F}_{TR} + \mathbf{F}_{FUS} - \mathbf{T}_I^B \mathbf{F}_T \right) - {}^B \mathbf{S}(\boldsymbol{\omega}_B) \begin{Bmatrix} u \\ v \\ w \end{Bmatrix} \quad (25)$$

$$\begin{Bmatrix} \dot{p}_B \\ \dot{q}_B \\ \dot{r}_B \end{Bmatrix} = \mathbf{I}_B^{-1} \left(\mathbf{M}_{\text{MR}} + \mathbf{M}_{\text{TR}} - {}^B S(\mathbf{r}_{cg}^{ct}) \mathbf{T}_I^B \mathbf{F}_T - {}^B \mathbf{S}(\boldsymbol{\omega}_B) \mathbf{I}_B \begin{Bmatrix} p_B \\ q_B \\ r_B \end{Bmatrix} \right) \quad (26)$$

where \mathbf{r}_{cg}^{ct} is the position vectors from the rotorcraft mass center to the tether connection, \mathbf{I}_B is the rotorcraft inertia matrix, and the common convention is used that a cross product of any vector \mathbf{r} with components r_x , r_y , and r_z expressed in a frame C is written:

$$\mathbf{r} \times = {}^C \mathbf{S}(\mathbf{r}) = \begin{bmatrix} 0 & -r_z & r_y \\ r_x & 0 & -r_x \\ -r_y & r_x & 0 \end{bmatrix} \quad (27)$$

IV. Recursive Tether Model

The tether configuration in Fig. 1 has spherical joints connecting the N slender bodies with no applied twisting torque at the ground or terminal link. The combination results in the spinning dynamics of each body having a minimal affect of the tether's overall motion. Elimination of tether spin will later aid in efficient computation of recursive dynamics. Angular velocity of the j^{th} body with respect to the inertial frame of reference is then defined as

$$\boldsymbol{\omega}_{j/I} = q_j \mathbf{j}_j + r_j \mathbf{k}_j \quad (28)$$

where the spin rate p_j is zero. The angular velocity of the j^{th} link, $\boldsymbol{\omega}_{j/I}$, may also be written as the sum of the previous body's angular velocity and the relative angular velocity of the j^{th} link and its preceding link $\boldsymbol{\omega}_{j/j-1}$:

$$\boldsymbol{\omega}_{j/I} = \boldsymbol{\omega}_{j/j-1} + \mathbf{T}_{j-1}^j \boldsymbol{\omega}_{j-1/I} \quad (29)$$

with $\boldsymbol{\omega}_{j/j-1}$ expressed in the b_j frame. Equation (29) can equivalently be expressed in component form

$$\boldsymbol{\omega}_{j/I} = \begin{Bmatrix} \omega_{xj} \\ \omega_{yj} \\ \omega_{zj} \end{Bmatrix} + \mathbf{T}_{j-1}^j \begin{Bmatrix} q_{j-1} \\ r_{j-1} \end{Bmatrix} = \begin{Bmatrix} 0 \\ q_j \\ r_j \end{Bmatrix} \quad (30)$$

where ω_{xj} , ω_{yj} , and ω_{zj} are the components of the relative angular velocity $\boldsymbol{\omega}_{j/j-1}$. Equation (30) can be separated into two portions, first the requirement that

$$\omega_{xj} = -\tilde{\mathbf{T}}_{j-1}^j \begin{Bmatrix} q_{j-1} \\ r_{j-1} \end{Bmatrix} \quad (31)$$

where $\tilde{\mathbf{T}}_{j-1}^j$ is a 1 x 2 sub matrix formed from the second and third elements of the first row of \mathbf{T}_{j-1}^j , and

$$\tilde{\boldsymbol{\omega}}_{j/I} = \begin{Bmatrix} \omega_{yj} \\ \omega_{zj} \end{Bmatrix} + \hat{\mathbf{T}}_{j-1}^j \begin{Bmatrix} q_{j-1} \\ r_{j-1} \end{Bmatrix} = \begin{Bmatrix} q_j \\ r_j \end{Bmatrix} \quad (32)$$

where $\hat{\mathbf{T}}_{j-1}^j$ is a 2 x 2 sub matrix formed from the second and third columns of the second and third rows of \mathbf{T}_{j-1}^j . A special case occurs at the root link b_1 because for the ground b_0 , both q_0 and r_0 are zero, so that $\omega_{x1}=0$ and

$$\tilde{\boldsymbol{\omega}}_{I/I} = \begin{Bmatrix} \omega_{y1} \\ \omega_{z1} \end{Bmatrix} = \begin{Bmatrix} q_1 \\ r_1 \end{Bmatrix} \quad (33)$$

Differentiation of the angular velocity with respect to the inertial frame results in the angular acceleration of the j^{th} body taking the recursive form

$$\boldsymbol{a}_{j/I} = \dot{\boldsymbol{\omega}}_{j/j-1} + \boldsymbol{\omega}_{j/I} \times \boldsymbol{\omega}_{j/j-1} + \mathbf{T}_{j-1}^j \boldsymbol{a}_{j-1/I} \quad (34)$$

where $\dot{\boldsymbol{\omega}}_{j/j-1}$ is the angular acceleration of b_j with respect to b_{j-1} expressed in the b_j frame. Expansion of (34) into matrix form results in

$$\boldsymbol{a}_{j/I} = \begin{Bmatrix} 0 \\ \dot{q}_j \\ \dot{r}_j \end{Bmatrix} = \begin{Bmatrix} \dot{\omega}_{xj} \\ \dot{\omega}_{yj} \\ \dot{\omega}_{zj} \end{Bmatrix} + \begin{Bmatrix} -r_j \omega_{yj} + q_j \omega_{zj} \\ r_j \omega_{xj} \\ -q_j \omega_{xj} \end{Bmatrix} + \mathbf{T}_{j-1}^j \begin{Bmatrix} 0 \\ \dot{q}_{j-1} \\ \dot{r}_{j-1} \end{Bmatrix} \quad (35)$$

The first row of (35) is automatically satisfied by (31). Substitution of (31) into the remaining two equations results in

$$\tilde{\boldsymbol{a}}_{j/I} = \begin{Bmatrix} \dot{q}_j \\ \dot{r}_j \end{Bmatrix} = \begin{Bmatrix} \dot{\omega}_{yj} \\ \dot{\omega}_{zj} \end{Bmatrix} - \begin{Bmatrix} r_j \\ -q_j \end{Bmatrix} \mathbf{T}_{j-1}^j \begin{Bmatrix} q_{j-1} \\ r_{j-1} \end{Bmatrix} + \hat{\mathbf{T}}_{j-1}^j \begin{Bmatrix} \dot{q}_{j-1} \\ \dot{r}_{j-1} \end{Bmatrix} \quad (36)$$

which can be written compactly as

$$\tilde{\boldsymbol{a}}_{j/I} = \dot{\boldsymbol{\omega}}_j + \boldsymbol{\lambda}_j + \hat{\mathbf{T}}_{j-1}^j \tilde{\boldsymbol{a}}_{j-1/I} \quad (37)$$

$$\boldsymbol{\lambda}_j = \begin{Bmatrix} r_j \\ -q_j \end{Bmatrix} \mathbf{T}_{j-1}^j \begin{Bmatrix} q_{j-1} \\ r_{j-1} \end{Bmatrix} \quad (38)$$

where $\dot{\boldsymbol{\omega}}_j = \begin{Bmatrix} \dot{\omega}_{yj} & \dot{\omega}_{zj} \end{Bmatrix}^T$.

Acceleration of the j^{th} body's mass center, \boldsymbol{a}_j^m , and acceleration of the j^{th} connection joint, \boldsymbol{a}_j^c , for $j = 0$ to $(N-1)$ can be written in the b_j frame as

$$\boldsymbol{a}_j^m = \mathbf{T}_{j-1}^j \boldsymbol{a}_{j-1}^c + \boldsymbol{a}_{j/I} \times \boldsymbol{r}_j^m + \boldsymbol{\omega}_{j/I} \times \boldsymbol{\omega}_{j/I} \times \boldsymbol{r}_j^m \quad (39)$$

$$\boldsymbol{a}_j^c = \mathbf{T}_{j-1}^j \boldsymbol{a}_{j-1}^c - \boldsymbol{r}_j^c \times \boldsymbol{a}_{j/I} + \boldsymbol{\omega}_{j/I} \times \boldsymbol{\omega}_{j/I} \times \boldsymbol{r}_j^c \quad (40)$$

where it is noted that $\boldsymbol{a}_0^c = 0$ since joint zero is attached to the ground.

The angular acceleration components of b_j (37) and acceleration of the $j-1$ joint (40) can be combined into a 5×1 acceleration vector $\dot{\mathbf{v}}_j = \{ \tilde{\boldsymbol{a}}_{j/I} \ \boldsymbol{a}_{j-1}^c \}^T$ and written

$$\dot{\mathbf{v}}_j = \mathbf{D}_j \dot{\mathbf{v}}_{j-1} + \mathbf{G}_j \dot{\boldsymbol{\omega}}_j + \boldsymbol{\Lambda}_j \quad (41)$$

where

$$\mathbf{D}_j = \begin{bmatrix} \hat{\mathbf{T}}_{j-1}^j & 0 \\ (\hat{\mathbf{S}}_j^c)^T & \mathbf{T}_{j-2}^{j-1} \end{bmatrix}, \quad \mathbf{G}_j = \begin{bmatrix} \mathbf{E}_2 \\ 0 \end{bmatrix} \quad (42)$$

$$\boldsymbol{\Lambda}_j = \begin{bmatrix} \boldsymbol{\lambda}_j \\ \boldsymbol{\omega}_{j-1/I} \times \boldsymbol{\omega}_{j-1/I} \times \boldsymbol{r}_{j-1}^c \end{bmatrix}, \quad \hat{\mathbf{S}}_j^c = \begin{bmatrix} 0 & 0 & -x_{cj} \\ 0 & x_{cj} & 0 \end{bmatrix} \quad (43)$$

A. Terminal Body Recursive Dynamics

The necessary dynamic equations for the tether model are formed using a Newtonian approach. A total of $2N$ vector equations are assembled where these equations will consist of N force equations and N moment equations. Forces on each body include weight, \mathbf{W}_j , and an external force \mathbf{F}_{Dj} , associated with it, both defined in the inertial frame. In addition, a reaction force $-\mathbf{R}_j$ on body b_j , defined in the b_j frame, occurs at the j^{th} joint for all j except for the terminal body. An equal, but opposite reaction \mathbf{R}_j is present on body b_{j+1} . A moment $-\mathbf{L}_j$ on body b_j , also defined in the b_j frame, occurs at the j^{th} joint for all j except for the terminal body. An equal but opposite moment \mathbf{L}_j is also present on body b_{j+1} . Neglecting spin dynamics requires that the moment \mathbf{L}_j cannot impart a twisting moment i.e. internal joint moments are only from relative link bending and bending rates. The terminal link also has an external load F_T from the visco-elastic element applied at the end of the terminal body. Formation of the dynamic equations is achieved by summing forces and moments for individual links with the moment equation expressed in the j body frame and the force equation expressed in the $j-1$ body frame. The two vector equations can then be put in a recursive form where moving through the tether from the terminal link back toward the root link, equations for the $j-1$ links contain terms from the j^{th} link such that these relationships become coupled. The recursive dynamic equations are developed below first for a terminal link then for a non-terminal link.

Equating the time derivative of linear momentum with the summation of forces on the $j-1$ body frame for a terminal link j results in

$$\mathbf{R}_{j-1} + \mathbf{T}_I^{j-1} (\mathbf{F}_{Dj} + \mathbf{W}_j + \mathbf{F}_T) = m_j (\mathbf{T}_{j-1}^j)^T \mathbf{a}_j^m \quad (44)$$

Similarly, summing moments about the connection joint c_{j-1} for the terminal link and equating to the time derivative of angular momentum in the j body frame yields

$$\mathbf{r}_j^m \times \mathbf{T}_I^j (\mathbf{F}_{Dj} + \mathbf{W}_j) + \mathbf{r}_j^c \times \mathbf{T}_I^j \mathbf{F}_T + \mathbf{T}_{j-1}^j \mathbf{L}_{j-1} = (\mathbf{I}_j \mathbf{a}_{j/I} + \boldsymbol{\omega}_{j/I} \times \mathbf{I}_j \boldsymbol{\omega}_{j/I}) + \mathbf{r}_j^m \times m_j \mathbf{a}_j^m \quad (45)$$

The i component of both sides of the moment summation (45) reduce to zero due to each link being a body of revolution and the fact that the position vector from connection joint $j-1$ to the mass center of the terminal link is defined such that it only has an i component. The remaining equations for the terminal link are assembled into a 5×1 force vector, \mathbf{F}_j , arranged such that the first two equations represent the two nonzero components of the moment equation while the remaining three equations are components of the force equation (44). The force vector takes the form

$$\mathbf{F}_j = \mathbf{M}_j \dot{\mathbf{v}}_j + \boldsymbol{\Gamma}_T \quad (46)$$

where (39) is incorporated in to both (44) and (45) with the following definitions:

$$\mathbf{F}_j = \begin{Bmatrix} 0 \\ \mathbf{R}_{j-1} \end{Bmatrix}, \quad \mathbf{M}_j = \begin{bmatrix} \tilde{\mathbf{I}}_j - m_j \tilde{\mathbf{S}}_j^m \tilde{\mathbf{S}}_j^m & m_j \hat{\mathbf{S}}_j^m \mathbf{T}_{j-1}^j \\ m_j (\mathbf{T}_{j-1}^j)^T (\hat{\mathbf{S}}_j^m)^T & m_j \mathbf{E}_3 \end{bmatrix}, \quad (47)$$

$$\tilde{\mathbf{I}}_j = \begin{bmatrix} I_{yy} & 0 \\ 0 & I_{zz} \end{bmatrix}, \quad \tilde{\mathbf{S}}_j^m = \begin{bmatrix} 0 & -x_{mj} \\ x_{mj} & 0 \end{bmatrix}, \quad \hat{\mathbf{S}}_j^m = \begin{bmatrix} 0 & 0 & -x_{mj} \\ 0 & x_{mj} & 0 \end{bmatrix}, \quad (48)$$

$$\boldsymbol{\Gamma}_T = \begin{bmatrix} -\hat{\mathbf{S}}_j^m \mathbf{T}_I^j (\mathbf{F}_{Dj} + \mathbf{W}_j) - \hat{\mathbf{S}}_j^c \mathbf{T}_I^j \mathbf{F}_T - \hat{\mathbf{T}}_{j-1}^j \tilde{\mathbf{L}}_{j-1} \\ m_j (\mathbf{T}_{j-1}^j)^T (\boldsymbol{\omega}_{j/I} \times \boldsymbol{\omega}_{j/I} \times \mathbf{r}_j^m) - \mathbf{T}_I^{j-1} (\mathbf{F}_{Dj} + \mathbf{W}_j + \mathbf{F}_T) \end{bmatrix} \quad (49)$$

The terms $\mathbf{r}_j^m \times m_j (\boldsymbol{\omega}_{j/I} \times \boldsymbol{\omega}_{j/I} \times \mathbf{r}_j^m)$ and $\boldsymbol{\omega}_{j/I} \times \mathbf{I}_j \boldsymbol{\omega}_{j/I}$ from (45) vanish due to the fact that the position vector from connection joint $j-1$ to the mass center of the terminal link is defined such that it only has only an i component, the links are bodies of revolution, and the spin rate in (28) is zero.

Substituting (31), the kinematic relationship for the acceleration vector, $\dot{\mathbf{v}}_j$ into (46) gives a relationship for the force vector, \mathbf{F}_j , in terms of the relative angular acceleration vector, $\dot{\boldsymbol{\omega}}_j$, expressed as

$$\mathbf{F}_j = \mathbf{M}_j (\mathbf{D}_j \dot{\mathbf{v}}_{j-1} + \mathbf{G}_j \dot{\boldsymbol{\omega}}_j + \boldsymbol{\Lambda}_j) + \boldsymbol{\Gamma}_T \quad (50)$$

The relative angular acceleration vector, $\dot{\boldsymbol{\omega}}_j$ is then found by premultiplying equation (50) by \mathbf{G}_j^T and noting that $\mathbf{G}_j^T \mathbf{F}_j = 0$:

$$\dot{\boldsymbol{\omega}}_j = -(\mathbf{G}_j^T \mathbf{M}_j \mathbf{G}_j)^{-1} \mathbf{G}_j^T (\mathbf{M}_j \mathbf{D}_j \dot{\mathbf{v}}_{j-1} + \mathbf{M}_j \boldsymbol{\Lambda}_j + \boldsymbol{\Gamma}_T) \quad (51)$$

Substitution of (51) and (41) into the force vector in (46) results in a final expression for the terminal body's force vector expressed only using its forces and the parent body's joint accelerations:

$$\mathbf{F}_j = \hat{\mathbf{M}}_j \mathbf{D}_j \dot{\mathbf{v}}_{j-1} + \hat{\boldsymbol{\Gamma}}_j \quad (52)$$

where

$$\mathbf{K}_j = \mathbf{M}_j \mathbf{G}_j (\mathbf{G}_j^T \mathbf{M}_j \mathbf{G}_j)^{-1} \quad (53)$$

$$\boldsymbol{\Gamma}_j^a = \boldsymbol{\Gamma}_T + \mathbf{M}_j \boldsymbol{\Lambda}_j \quad (54)$$

$$\hat{\boldsymbol{\Gamma}}_j = \boldsymbol{\Gamma}_j^a - \mathbf{K}_j \mathbf{G}_j^T \boldsymbol{\Gamma}_j^a \quad (55)$$

$$\hat{\mathbf{M}}_j = \mathbf{M}_j - \mathbf{K}_j \mathbf{G}_j^T \mathbf{M}_j \quad (56)$$

B. Non-terminal Body Recursive Dynamics

Following similar steps as outlined above for the terminal link, vector equations for the non-terminal links can be formed. The forces are summed on each of these links while moments are summed about the c_{j-1} connection joint for each j^{th} link in the tether. Again, the moment equations are expressed in the j body frame while the force equations are expressed in the $j-1$ body frame. All non-terminal links can be shown to have an equivalent recursive form

$$\mathbf{R}_{j-1} - (\mathbf{T}_{j-1}^j)^T \mathbf{R}_j + \mathbf{T}_I^{j-1} (\mathbf{F}_{Dj} + \mathbf{W}_j) = m_j (\mathbf{T}_{j-1}^j)^T \mathbf{a}_j^m \quad (57)$$

by summing forces and equating to the linear momentum. The moment equation then takes the form

$$\begin{aligned} & \mathbf{r}_j^m \times \mathbf{T}_I^j (\mathbf{F}_{Dj} + \mathbf{W}_j) - \mathbf{r}_j^c \times \mathbf{R}_j + \mathbf{T}_{j-1}^j \mathbf{L}_{j-1} - \mathbf{L}_j \\ &= (\mathbf{I}_j \mathbf{a}_{j/I} + \boldsymbol{\omega}_{j/I} \times \mathbf{I}_j \boldsymbol{\omega}_{j/I}) + \mathbf{r}_j^m \times m_j \mathbf{a}_j^m \end{aligned} \quad (58)$$

Equations (57) and (58) may now be assembled into matrix form in a similar fashion to that of the terminal link. The i component of the moment equation vanishes and the matrix form reduces to a 5×1 system. Non-terminal links all have the equivalent form

$$\mathbf{F}_j = \mathbf{M}_j \dot{\mathbf{v}}_j + \boldsymbol{\Gamma}_j + \mathbf{D}_{j+1}^T \mathbf{F}_{j+1} \quad (59)$$

with

$$\mathbf{\Gamma}_j = \begin{bmatrix} -\hat{\mathbf{S}}_j^m \mathbf{T}_I^j (\mathbf{F}_{Dj} + \mathbf{W}_j) - \hat{\mathbf{T}}_{j-1}^j \tilde{\mathbf{L}}_{j-1} + \tilde{\mathbf{L}}_j \\ m_j (\mathbf{T}_{j-1}^j)^T (\boldsymbol{\omega}_{j/I} \times \boldsymbol{\omega}_{j/I} \times \mathbf{r}_j^m) - \mathbf{T}_I^{j-1} (\mathbf{F}_{Dj} + \mathbf{W}_j) \end{bmatrix} \quad (60)$$

where the terms $\mathbf{r}_j^m \times m_j (\boldsymbol{\omega}_{j/I} \times \boldsymbol{\omega}_{j/I} \times \mathbf{r}_j^m)$ and $\boldsymbol{\omega}_{j/I} \times \mathbf{I}_j \boldsymbol{\omega}_{j/I}$ become zero just as with the terminal link. The force vector (59) for the j^{th} body is coupled to the force vector from the previous link by the term $\mathbf{D}_{j+1}^T \mathbf{F}_{j+1}$. It can be shown that the force vector for any non-terminal link can be written just as the terminal link (52) where it depends on its forces and the parent body's joint accelerations. Consider (59) for the terminal link's parent. Substitution of the terminal link force vector (52) into (59) results in

$$\mathbf{F}_j = \tilde{\mathbf{M}}_j \dot{\mathbf{v}}_j + \tilde{\mathbf{\Gamma}}_j \quad (61)$$

where

$$\tilde{\mathbf{M}}_j = \mathbf{M}_j + \mathbf{D}_{j+1}^T \hat{\mathbf{M}}_{j+1} \mathbf{D}_{j+1} \quad (62)$$

$$\tilde{\mathbf{\Gamma}}_j = \mathbf{\Gamma}_j + \mathbf{D}_{j+1}^T \hat{\mathbf{\Gamma}}_{j+1} \quad (63)$$

Substitution of (41) into (61) gives a relationship for the force vector, \mathbf{F}_j , in terms of the relative angular acceleration vector, $\dot{\boldsymbol{\omega}}_j$. Similar to the terminal link, multiplying the result by \mathbf{G}_j^T and noting that $\mathbf{G}_j^T \mathbf{F}_j = 0$, $\dot{\boldsymbol{\omega}}_j$ for non-terminal links takes the form

$$\dot{\boldsymbol{\omega}}_j = -(\mathbf{G}_j^T \tilde{\mathbf{M}}_j \mathbf{G}_j)^{-1} \mathbf{G}_j^T (\tilde{\mathbf{M}}_j \mathbf{D}_j \dot{\mathbf{v}}_{j-1} + \mathbf{\Gamma}_j^a) \quad (64)$$

where

$$\mathbf{\Gamma}_j^a = \tilde{\mathbf{\Gamma}}_j + \tilde{\mathbf{M}}_j \boldsymbol{\Lambda}_j \quad (65)$$

The non-terminal link force vector then takes the form

$$\mathbf{F}_j = \hat{\mathbf{M}}_j \mathbf{D}_j \dot{\mathbf{v}}_{j-1} + \hat{\mathbf{\Gamma}}_j \quad (66)$$

by combining (41) and (64) with (61) and defining,

$$\mathbf{K}_j = \tilde{\mathbf{M}}_j \mathbf{G}_j (\mathbf{G}_j^T \tilde{\mathbf{M}}_j \mathbf{G}_j)^{-1} \quad (67)$$

$$\hat{\mathbf{\Gamma}}_j = \mathbf{\Gamma}_j + \tilde{\mathbf{M}}_j \boldsymbol{\Lambda}_j - \mathbf{K}_j \mathbf{G}_j^T \mathbf{\Gamma}_j^a \quad (68)$$

$$\hat{\mathbf{M}}_j = \tilde{\mathbf{M}}_j - \mathbf{K}_j \mathbf{G}_j^T \tilde{\mathbf{M}}_j \quad (69)$$

C. Solution Procedure

The recursive solution begins with a backward pass through the tether system starting at the terminal link. At the terminal link ($j = N$) the force vector, \mathbf{F}_j in (46) and (52) can be formed. Formation of force vectors for all non-terminal links then follows for $j = N-1$ to 1 using (61) and (66). Upon reaching the root link ($j = 1$), the acceleration vector $\dot{\mathbf{v}}_1$ in (61) becomes solvable. Since the root link is attached to the ground, \mathbf{a}_0^e is zero and the solution to $\tilde{\mathbf{a}}_{1/I}$ only requires the inversion of a 2 x 2 matrix. Therefore, at the

end of the backwards pass the solution to $\dot{\mathbf{v}}_I$ is found. Once the acceleration vector, $\dot{\mathbf{v}}_I$, for the root link is known, a forward pass is used to find the angular acceleration vector, $\dot{\boldsymbol{\omega}}_j$, and the acceleration vector, $\dot{\mathbf{v}}_j$, using (64) and (41) for $j = 2$ to $N-1$ then (51) and (41) for $j = N$. Completion of the forward pass results in the solution to the N angular accelerations, $\tilde{\boldsymbol{\alpha}}_{j/I}$, for $j = 1$ to N required for numerical integration.

V. Simulations

A. System Parameters

In order to demonstrate application of the proposed model and it's utility in analyzing the rotorcraft and tether dynamics along with tether loads, simulations of an example TREX 600 rotorcraft with a 50m of tether are shown. Characteristics of the rotorcraft are provided below in Table 1. The tether has a 4 mm diameter, total mass of 0.6 kg, and is divided into 9 segments with joint damping coefficient being 0.017 N-s. The visco-elastic element has an unstretched length, L_{ve} , of 1m and K_s , K_v , and C_v of 175 N/m, 400 N/m, and 40 N-s/m, respectively.

Table 1. Rotorcraft Parameters

Parameter	Value	Units
I_{XX}	0.135	$kg \cdot m^2$
I_{YY}	0.263	$kg \cdot m^2$
I_{ZZ}	0.210	$kg \cdot m^2$
m	3.3	kg
R_{MR}	0.68	m
c_{MR}	0.057	m
h_z	0.305	m
l_{ir}	-0.80	m
C_{D0}	0.01	-
a	5.5	$1/rad$
Ω_{MR}	158	rad/s
$\partial\alpha/\partial\mu_x$	-0.01	rad
$\partial\beta/\partial\mu_y$	0.01	rad
K_{LAT}, K_{LON}	0.8	-
k	45	$N \cdot m/rad$
τ	0.09	sec
C_{DX}, C_{DY}, C_{DZ}	0.2	-

B. Rotorcraft Controller

During the simulation the rotorcraft tracks a desired position and orientation. In hover the desired altitude simply becomes the desired height above ground. Desired roll and pitch are related to the position of the helicopter. Figure 2 shows a top view of a helicopter with a desired hover location. A vector \mathbf{r} describing the position error in the helicopter frame is defined in (70). Equations (71) and (72) relate the

desired roll and pitch to the desired location through terms proportional to the position and velocity errors. Desired roll also includes a constant to compensate for tail thrust.

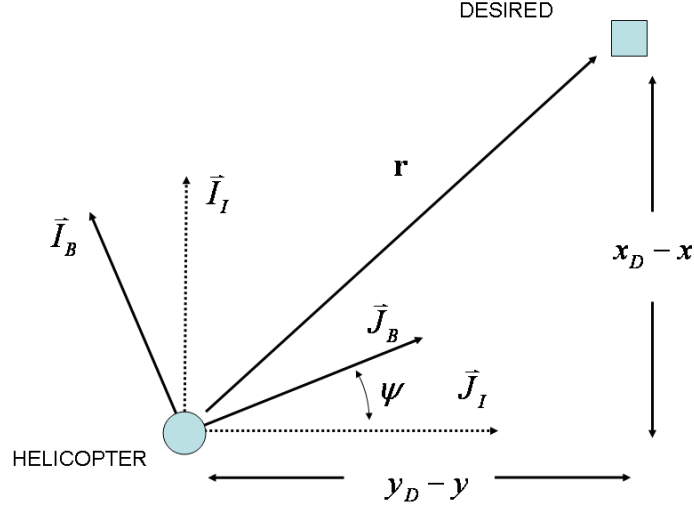


Fig. 2 Desired Roll and Pitch Geometry

$$\mathbf{r} = \begin{Bmatrix} r_x \\ r_y \\ 0 \end{Bmatrix} = \begin{bmatrix} c_\psi & s_\psi & 0 \\ -s_\psi & c_\psi & 0 \\ 0 & 0 & 1 \end{bmatrix} \begin{Bmatrix} x_D - x \\ y_D - y \\ 0 \end{Bmatrix} \quad (70)$$

$$\phi_{DES} = -K_p r_y + K_D \dot{r}_y + K_{\phi ss} \quad (71)$$

$$\theta_{DES} = K_p r_x - K_D \dot{r}_x \quad (72)$$

The four control inputs for the rotorcraft are then determined by a simple PID controller according to:

$$\begin{aligned} u_{lat} &= K_{p\phi}(\phi_B - \phi_{DES}) + K_{D\phi} \dot{\phi}_B \\ u_{lon} &= K_{p\theta}(\theta_B - \theta_{DES}) + K_{D\theta} \dot{\theta}_B \\ u_{col} &= K_{z0} + K_{pz}(z - z_{DES}) + K_{Dz} \dot{z} \\ T_{TR} &= K_{\psi 0} + K_{p\psi}(\psi_B - \psi_{DES}) + K_{D\psi} \dot{\psi}_B \end{aligned} \quad (73)$$

C. Tethered Rotorcraft Simulations

In the initial simulation, the rotorcraft is initially directly above the ground connection and the tether vertical. Orientation of the rotorcraft is initially facing in the opposite direction of i_I with ψ_B being π . Rotorcraft, visco-elastic, and recursive tether differential equations are numerically integrated using a fourth order Runge-Kutta algorithm with time step of 0.02 seconds. Gains for desired roll and pitch $K_p, K_D, K_{\phi ss}$ where selected as 0.007, 0.07 and 0.03 rad, respectively. The remaining PID gains are provided in Table 2. The desired position is $x = 10\text{m}$, $y = 0\text{m}$, $z = 47\text{m}$ and the desired orientation is $\phi = \theta = 0\text{ deg}$ and $\psi = \pi\text{ deg}$.

Table 2. PID Gains	
Gain	Value
$K_{P\phi}$	-0.05
$K_{D\phi}$	-0.004
$K_{P\theta}$	-0.05
$K_{D\theta}$	-0.004
K_{z0}	0.148
K_{Pz}	0.02
K_{Dz}	0.006
$K_{\psi0}$	-1.07
$K_{P\psi}$	1.0
$K_{D\psi}$	0.5

Figures 3 and 4 show the trajectory for a 35 second simulation while Fig. 5 shows the tether orientation at the final time of 35 seconds. Tension in the tether at the connection point is shown in Fig. 6. Initially as the rotorcraft descends the tension reduces until at approximately 8 seconds the rotorcraft stops descending and the tension increases as the tether's momentum is stopped. Also high frequency dynamics can be seen as the tether tension changes. The rotorcraft controls, orientation, and angular velocities are shown in Figs. 7, 8, and 9.

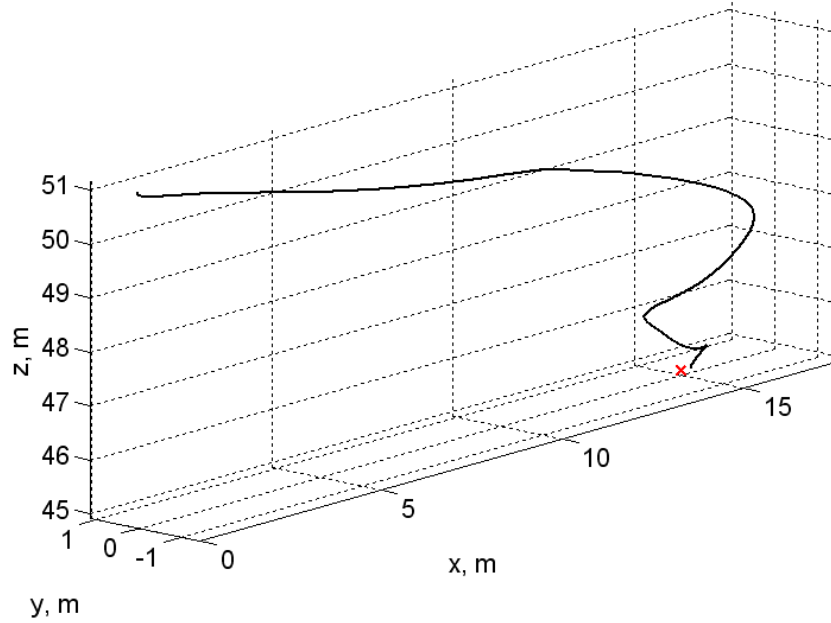


Figure 3. 3-D tethered rotorcraft CG position.

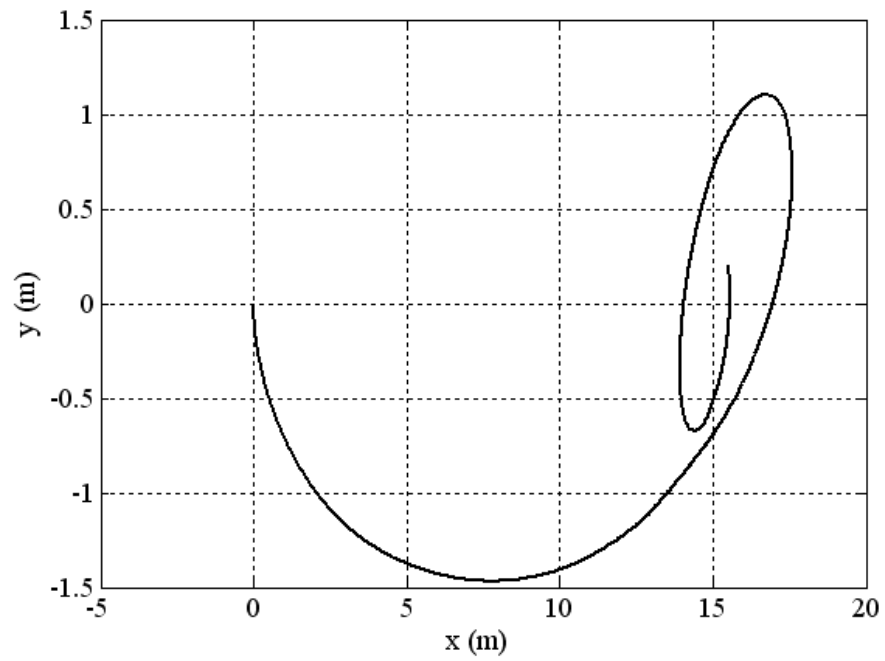


Figure 4. Horizontal view of rotorcraft CG.

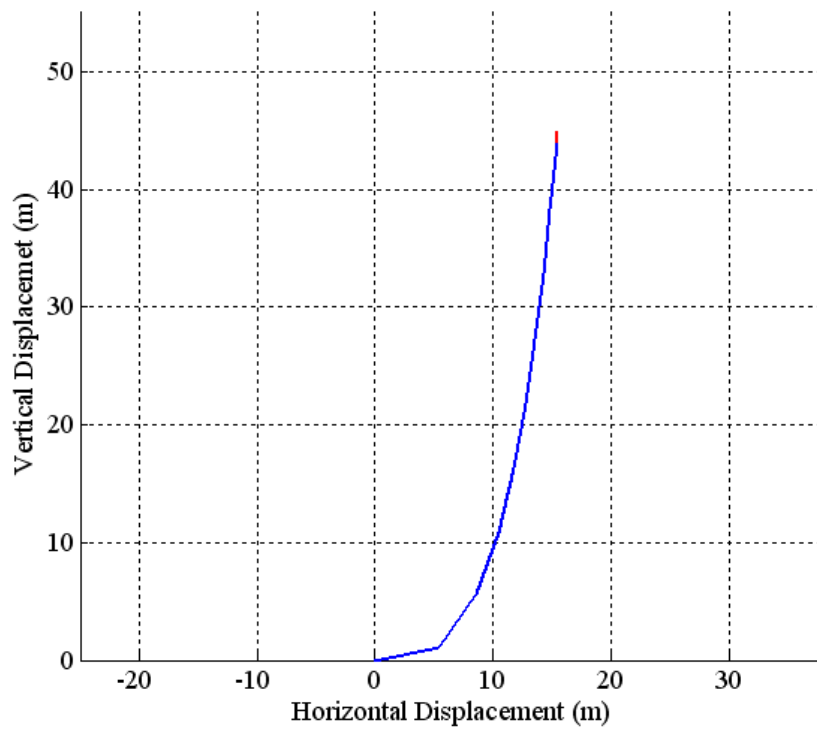


Figure 5. Final 9-link tether orientation.

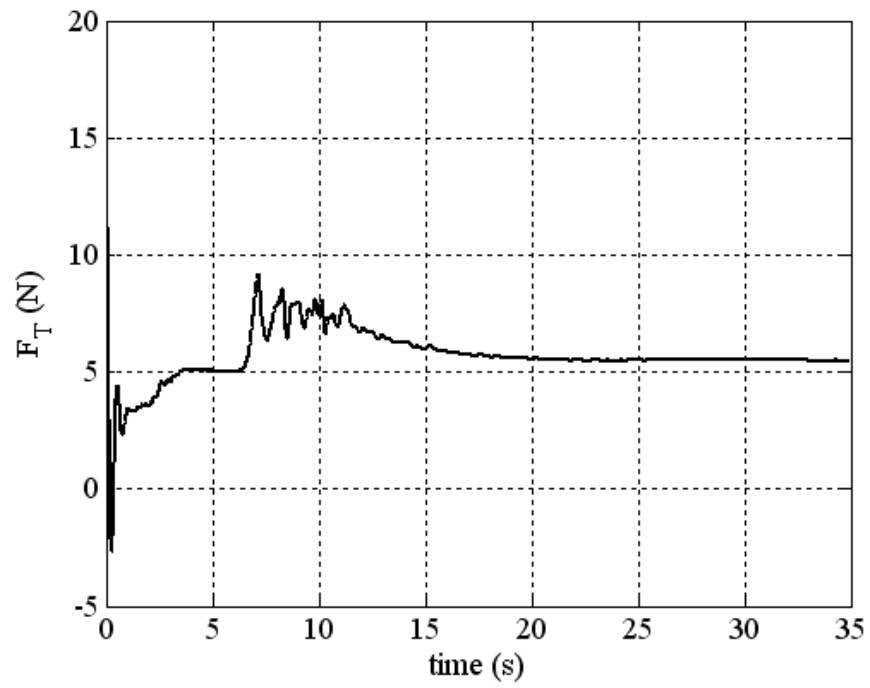


Figure 6. Visco-elastic tension.

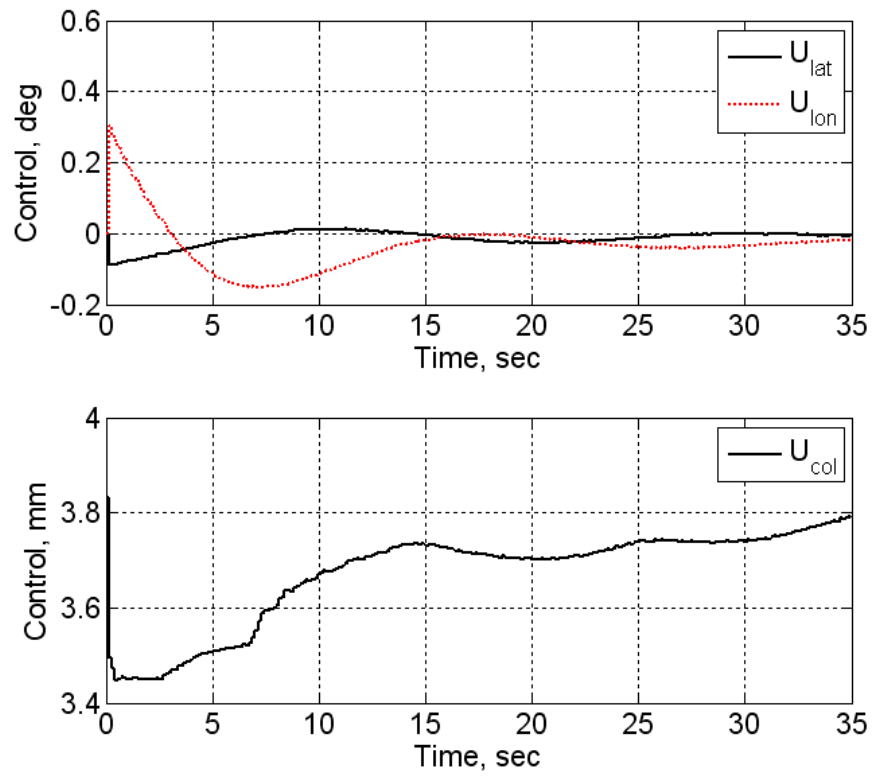


Figure 7. Rotorcraft controls.

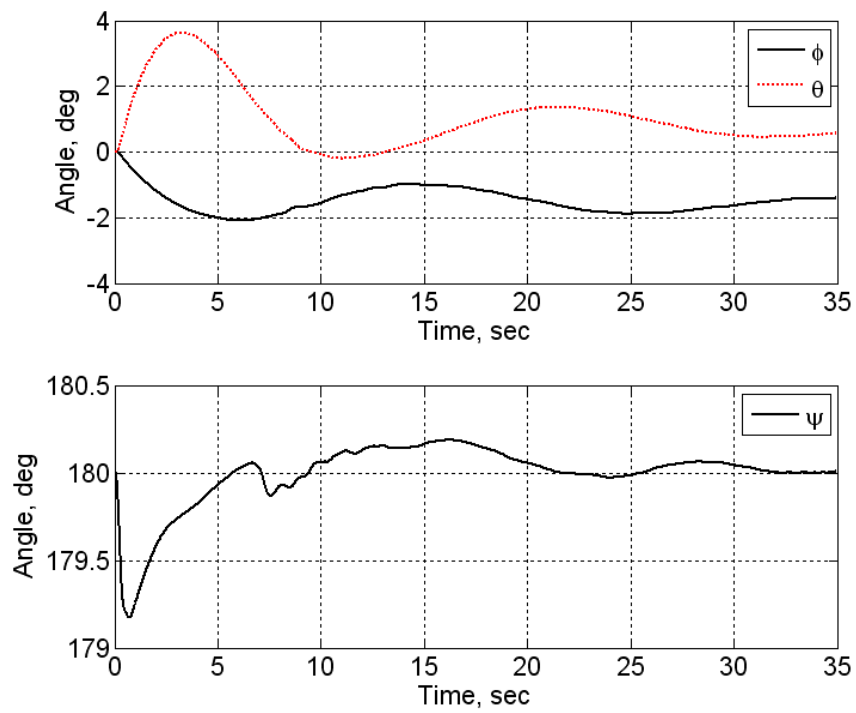


Figure 8. Rotorcraft Euler angles.

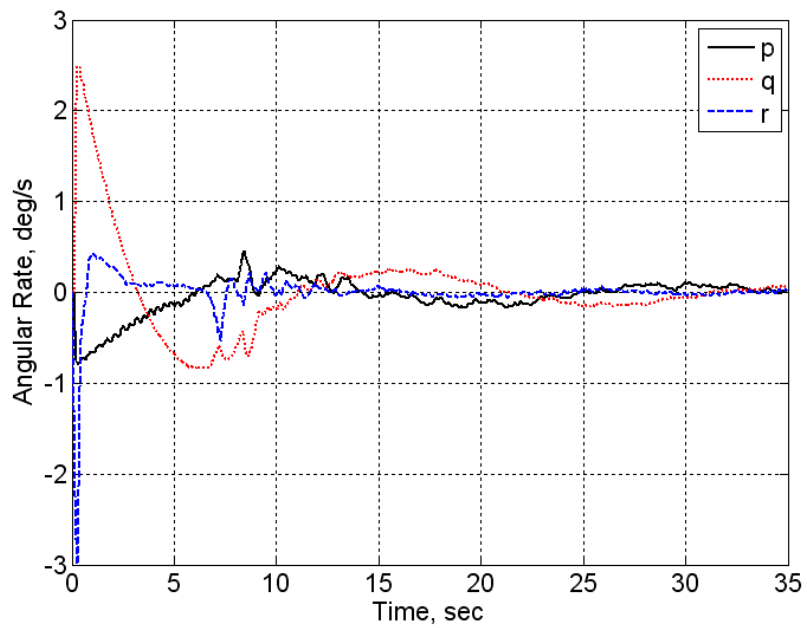


Figure 9. Rotorcraft angular velocities.

References

- ¹Kang, W., and Lee, I., "Analysis of tethered Aerostat Response Under Atmospheric Turbulence Considering nonlinear Cable Dynamics," *Journal of Aircraft*, Vol. 46, No. 1, 2009, pp. 343-347.
- ²Aglietti, G., "Dynamic Response of a High-Altitude Tethered Balloon System," *Journal of Aircraft*, Vol. 46, No. 6, 2009, pp. 2032-2040.
- ³Nahon, M., Gilardi, G., and Lambert, C. "Dynamics/Control of a Radio Telescope Receiver Supported by a Tethered Aerostat," *Journal of Guidance, Control, and Dynamics*, Vol. 25, No. 6, 2002, pp. 1107-1115.
- ⁴Lambert, C., Nahon, M., and Chalmers, D., Gilardi, G., "Cable Control of an Aerostat Platform: Experimental Results and Model Validation," *Journal of Guidance, Control, and Dynamics*, Vol. 30, No. 2, 2007, pp. 620-628.
- ⁵Frost, G., and Costello, M., "Improved Deployment Characteristics of a Tether-Connected Munition System," *Journal of Guidance, Control, and Dynamics*, Vol. 24, No. 3, 2001, pp. 547-554.
- ⁶Kyle, J., and Costello, M., "Comparison of Measured and Simulated Motion of a Scaled Dragline Excavation System," *Mathematical and Computer Modelling*, Vol. 44, No. 4, 2006, pp. 816-833.
- ⁷Jerkovsky, W., "The Structure of Multibody Dynamic Equations," *Journal of Guidance, Control, and Dynamics*, Vol. 1, No. 3, 1978, pp. 173-182.
- ⁸Kane, T., Linkins, P., and Levinson, D., *Spacecraft Dynamics, d Dynamics*, McGraw-Hill., New York, 1983.
- ⁹Hollerbach, J., "A Recursive Lagrangian Formulation of Manipulator Dynamics and a Comparative Study of Dynamic Formulation Complexity," *IEEE Transactions on Systems, Man, and, Cybernetics*, Vol. 10, No. 11, 1980, pp. 730-736.
- ¹⁰Schielen, W., "Computational Dynamics: Theory and Application of Multibody Systems," *Eur. J. Mech. A/Solids*, Vol. 25, 2006, pp 566-594.
- ¹¹Kuipers, J., *Quaternions and Rotation Sequences*, Princeton University Press, New Jersey 1999, pp. 103–136.
- ¹²Gavrilets, V., Mettker, B., and Feron, E., "Nonlinear Model for a Small-Size Acrobatic Helicopter," *Proceedings of AIAA Guidance, Navigation, and Control Conference*, AIAA, Reston, VA, 2001.
- ¹³Padfield, G., Helicopter Flight dynamics: The Theory and Application of Flying Qualities and Simulation Modeling, AIAA Education Series, 1995.